IEEE Transactions on Nuclear Science, **44**(6):2473–2476, 1997 (preprint)

Automated 3-D Segmentation of Respiratory-Gated PET Transmission Images

BW Reutter, *Member, IEEE*, GJ Klein, *Member, IEEE*, and RH Huesman, *Member, IEEE*
Center for Functional Imaging, Lawrence Berkeley National Laboratory
University of California, One Cyclotron Road, Berkeley, CA 94720

Abstract

As a preliminary step toward performing respiration compensated attenuation correction of respiratory-gated cardiac PET data, we acquired and automatically segmented respiratory-gated transmission data for a dog breathing on its own under gas anesthesia.

Transmission data were acquired for 20 min on a CTI/Siemens ECAT EXACT HR (47-slice) scanner. Two respiratory gates were obtained using data from a pneumatic bellows placed around the dog's chest. For each respiratory gate, torso and lung surfaces were segmented automatically using a differential 3-D image edge detection algorithm. Three-dimensional visualizations showed that during inspiration the heart translated about 4 mm transversely and the diaphragm translated about 9 mm inferiorly.

The observed respiratory motion of the canine heart and diaphragm suggests that respiration compensated attenuation correction may be necessary for accurate quantitation of high-resolution respiratory-gated human cardiac PET data. Our automated image segmentation results suggest that respiration compensated segmented attenuation correction may be possible using respiratory-gated transmission data obtained with as little as 3 min of acquisition time per gate.

I. INTRODUCTION

Over the past 20 years, the spatial resolution attainable by positron emission tomography (PET) systems has improved dramatically. With this improved resolution, there is the potential to obtain detailed maps of myocardial perfusion and metabolism. However, this potential remains largely unfulfilled since current data acquisition and analysis strategies do not account for the respiratory and contractile motion of the human heart, which has an amplitude more than twice the 4–5 mm resolution of contemporary commercial scanners. While the resulting blurred images are reasonable qualitative estimates of the left ventricular myocardial activity, they fall far short of the high-resolution quantitative images that are potentially attainable with modern PET systems.

The effects of respiratory motion of the heart have been virtually ignored in cardiac emission tomography, although the problem has been recognized and was described in 1982 [1]. Gross patient motion effects have been studied, however, particularly with respect to the misalignment that often results between PET transmission and emission data [2]–[4]. A 20 mm patient motion between transmission and emission scans produced changes of up to 30% in regional myocardial activity estimates [3]. Respiratory motion of the diaphragm and heart has been estimated to be approximately 15 mm in a supine human during tidal breathing [5]–[7]. Thus, the respiratory motion of the diaphragm and heart could significantly impact the quantitation of high-resolution gated cardiac emission data if ungated transmission data are used for attenuation correction.

In order to investigate methods for heart motion compensation, we have developed a technique for separating events during both transmission and emission data acquisition according to respiratory and electrocardiogram (EKG) cues. Emission data can then be analyzed using properly registered attenuation correction factors (ACFs).

When data acquired during a typical 20 min transmission study are separated into multiple respiratory states, however, the resulting ACFs for each state are noisy due to relatively low counting statistics. To obtain less noisy ACFs, methods have been developed to segment noisy transmission images into air, soft tissue, and lung based on semi-automatic differential-based 2-D edge detection [8], automatic threshold-based pixel classification [9]–[11], and neural network pattern classification [12]. This patient segmentation typically is smoothed with a Gaussian to obtain a map with resolution comparable to the emission data, and is then combined with a map for the tomograph bed obtained from a separate high-statistics transmission study performed without the patient in the scanner. The combined map is then forward-projected to obtain less noisy ACFs.

To supplement these methods, we have developed efficient differential 3-D image processing methods which automatically create time-varying geometric models of the torso and lung surfaces from noisy respiratory-gated transmission data. A pixel can then be classified according to which surface (if any) most immediately encloses the pixel during a given respiratory state, and assigned an appropriate attenuation coefficient corresponding to air, soft tissue, or lung.

II. HARDWARE GATING

In collaboration with CTI Inc. (Knoxville, TN), we modified the software and hardware of our CTI/Siemens ECAT EXACT HR (47-slice) tomograph to support prospective respiratory gating. The modified tomograph front panel accepts four TTL inputs which encode a desired acquisition gate. As these inputs change, tomograph events are directed to one of 12 different data buffers in memory, where each buffer contains the data from the 47 2-D slices acquired for that gate.

To supply the 4-bit gating address to the scanner, we implemented a hardware and software front end. The front end characterizes the respiratory state of the patient from external analog cues using the LabVIEW real-time environment (National Instruments, Austin, TX) on a Macintosh workstation (Apple Computer, Cupertino, CA), as well as custom analog signal processing hardware. Respiratory monitoring is achieved using a pneumatic bellows originally designed for magnetic resonance image (MRI) scanners (part number E8811ED: Bellows Assembly for Respiratory Compensation Packages, General Electric Medical Systems, Milwaukee, WI). The bellows is secured around the patient's chest, and the analog signal from a pressure transducer connected to the bellows is amplified and input to a National Instruments NB-MIO-16 data acquisition board resident in the Macintosh. The Macintosh samples the respiratory signal at 10 Hz. For each sample, a respiratory state is set based upon the absolute amplitude of the pressure transducer signal, and used to select an output gating state. This state is encoded by the National Instruments board as four binary outputs and directed to the ECAT scanner.

Using this gating configuration with two respiratory gates, a 20 min transmission study was performed on a dog breathing on its own under gas anesthesia. The respiratory gating threshold was placed near end-expiration to acquire a dataset at end-expiration and a dataset during inspiration. Only two respiratory gates were chosen because the anesthetized dog remained in the end-expiration state about 85% of the time, taking only occasional, relatively shallow, quick breaths.

III. Automated 3-D Transmission Image Segmentation

We implemented a 3-D edge detection operator that estimates the second derivative in the direction of the image intensity gradient, weighted by the squared gradient magnitude:

$$\|\nabla f\|^2 \left[\frac{\nabla f}{\|\nabla f\|} \cdot \nabla \left[\frac{\nabla f}{\|\nabla f\|} \cdot \nabla f\right]\right] = \sum_{p=1}^{3}\sum_{q=1}^{3} \frac{\partial f}{\partial (x^p)} \frac{\partial f}{\partial (x^q)} \frac{\partial^2 f}{\partial (x^p)\partial (x^q)}. \tag{1}$$

Here, x^1, x^2, and x^3 denote the spatial coordinates. For convenience, we will also denote these coordinates by x, y, and z, respectively. This operator and a similar second-order differential operator, the Laplacian $\nabla^2 f = \sum_{p=1}^{3} \frac{\partial^2 f}{\partial (x^p)^2}$, have been used in a number of medical imaging applications [13]–[16]. In 2-D, the second directional derivative operator has been shown to perform better than the Laplacian [17], [18].

Zero-crossing points in the second directional derivative output correspond to local extrema in the image intensity gradient magnitude. Among these are the points where locally the image intensity is changing relatively rapidly. These points lie on the boundaries or edges between relatively homogeneous regions delineated with adequate contrast. In particular, we are interested in automatically extracting and physically modeling the time-varying surfaces bounding the torso and the lungs.

Each respiratory-gated transmission dataset was composed of 47 contiguous 3.125 mm-thick transverse images reconstructed using standard filtered back-projection of the logarithm of an appropriately normalized ratio of the canine transmission dataset and a blank transmission dataset acquired with the field-of-view clear of all attenuating objects. Each transverse image was 128×128 pixels, with pixel size 2.5×2.5 mm. Due to the infrequent shallow breathing of the dog, the length of the data acquisition during inspiration totaled only about 3 min and yielded about 650k counts per transverse plane, while the length of the data acquisition during end-expiration totaled about 17 min and yielded about 3.4M counts per plane. Figures 1 and 2 show that compared to the end-expiration images, the inspiration images are noisier and have less homogeneous air, soft tissue, and lung regions.

We processed each 128×128×47 image dataset using the 3-D second directional derivative operator (Equation 1). The first-order and second-order partial derivatives needed to calculate Equation 1 were estimated efficiently by convolving the images with spline derivative filter kernels that smooth the images prior to performing differentiation [19].

Potentially interesting anatomical surfaces were constructed automatically after discarding the results from the first and last four transverse sections, which were excessively noisy due to boundary effects at the ends of the tomograph. Using an approach similar to Wallin [20], we linked together the zero-crossing points in the second directional derivative operator output. In each xy (transverse), xz (coronal), and yz (sagittal) image plane, bilinear interpolation was used to obtain sub-pixel spatial localization of the zero-crossing points. The zero-crossing points for each respiratory state were then linked together to form contours in each spatial plane. Surfaces were then constructed by linking together the contours. Information about the centroid, bounding box, and average image intensity gradient across each contour, as well as each surface, was stored to facilitate identifying the surfaces.

Figures 1 and 2 show the results of processing using kernels with supports 11×11×7 pixels (along the x, y, and z axes, respectively) and 23×23×15 pixels. Figure 1 shows that the heart translated about 4 mm transversely during inspiration. Figure 2 shows that the diaphragm translated about 9 mm inferiorly during inspiration.

Processing with the 11×11×7 kernel resulted in reasonably accurate torso and lung surface models, with some smaller-scale soft tissue areas mistakenly included as part of the lungs due to image noise. Processing with the 23×23×15 kernel eliminated most of the smaller-scale noise structures, but resulted in less accurate torso and lung surface models. Use of the 11×11×7 kernel appears to be preferable because of its more accurate localization of potentially interesting surfaces, provided that the effects of initially misclassifying soft tissue as lung can be mitigated. This is discussed further in Section V. With either kernel size, the relatively large, high-contrast, cross-sectional contours associated with the torso and lung surfaces were identified easily using the information stored about the centroid, bounding box, and average image intensity gradient across each contour. For a given filter kernel size, the 3-D differential image processing and automated surface construction took about 1.7 min for each respiratory state, on a 100 MHz R4000-based UNIX workstation (Silicon Graphics Inc., Mountain View, CA).

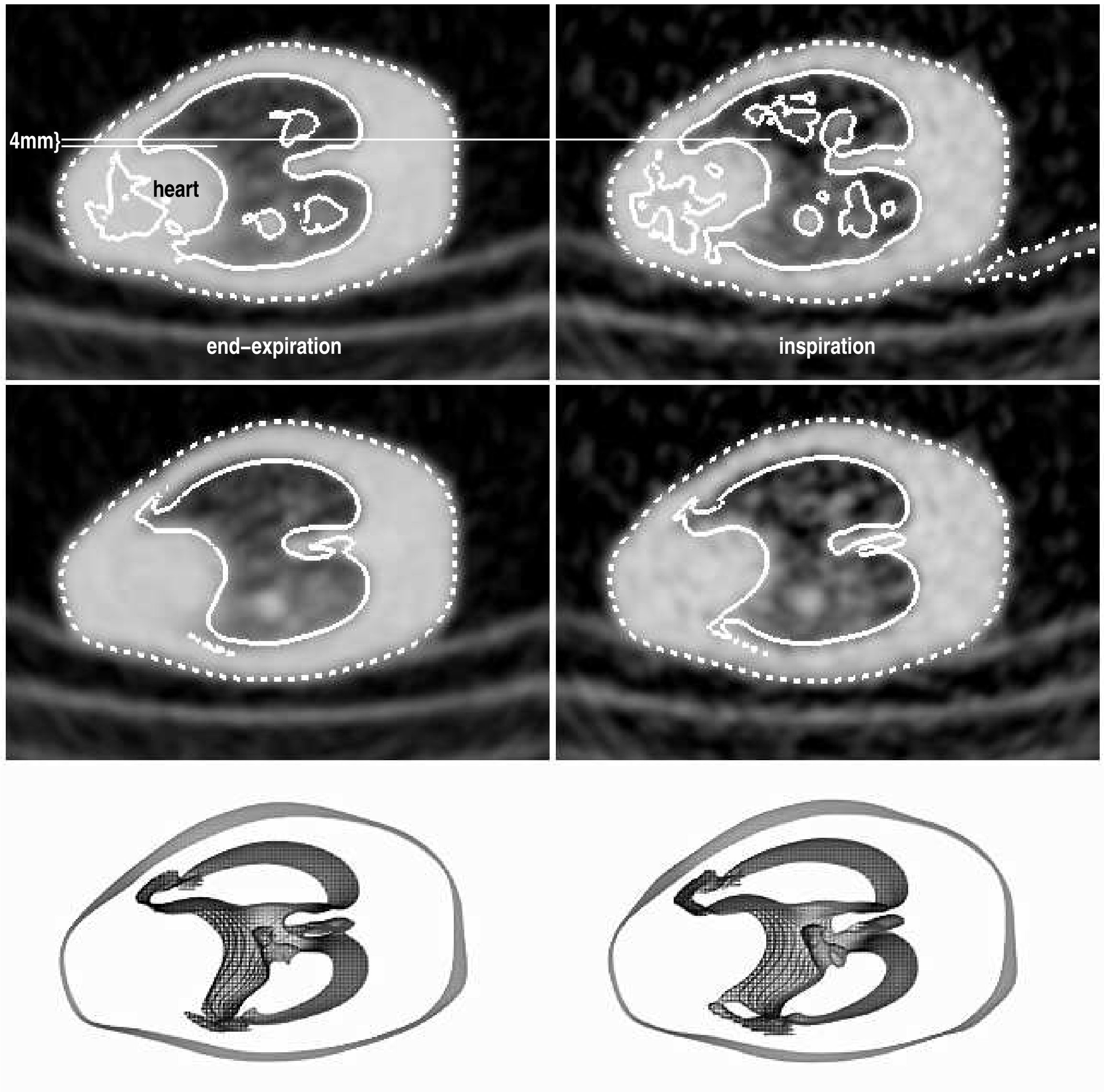

Fig. 1 Upper, Middle: Transverse respiratory-gated canine transmission images superimposed with cross-sections of torso (dashed contour) and lung (solid contour) surface models constructed automatically using the 3-D second directional derivative operator (upper left: end-expiration, $11\times11\times7$ operator; upper right: inspiration, $11\times11\times7$ operator; middle left: end-expiration, $23\times23\times15$ operator; middle right: inspiration, $23\times23\times15$ operator). The thin solid lines show that the heart translated about 4 mm transversely during inspiration. Lower: Inferior views of canine torso and lung surface models constructed automatically using the $23\times23\times15$ operator (lower left: end-expiration; lower right: inspiration). The dog is lying on its right side.

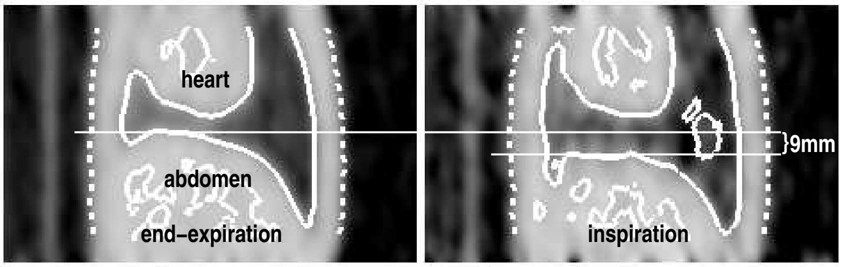

Fig. 2 Coronal respiratory-gated canine transmission images superimposed with cross-sections of torso (dashed contour) and lung (solid contour) surface models constructed automatically using the $11\times11\times7$ second directional derivative operator (left: end-expiration; right: inspiration). The thin solid lines show that the diaphragm translated about 9 mm inferiorly during inspiration.

IV. Conclusions

A strength of our automated differential image processing methods is that data are analyzed efficiently in 3-D over appropriate spatial scales in an effort to extract and to physically model the time-varying surfaces which bound the torso and lungs. Our structured analysis imposes spatial continuity constraints that complement the information which is available from unstructured image pixel gray-level value alone. Using these methods we obtained good 3-D segmentations of canine images reconstructed from respiratory-gated transmission data obtained with as little as 3 min of acquisition time per gate. The observed respiratory motion of the canine heart and diaphragm suggests that respiration compensated attenuation correction may be necessary for accurate quantitation of high-resolution respiratory-gated human cardiac PET data.

V. Future Directions

We have embarked on full 4-D structured analysis and validation of respiratory-gated human transmission data. Because an awake human breathes more regularly than does an anesthetized dog, sufficient data can be acquired during intermediate respiratory states to facilitate tracking the larger and more continuously varying motion of the diaphragm and heart. The acquisition of 4 or 5 respiratory gates during a typical 20 min transmission study will provide about 4 to 5 min of data per gate, which appears to be sufficient to yield good 3-D image segmentations. By processing in 4-D the data that we acquire using 4 or 5 respiratory gates, we expect that the additional temporal continuity constraint will aid the extraction and tracking of the torso and lung surfaces across both space and time.

Because attenuation within the lungs varies significantly between patients, as well as spatially and with respiratory phase [11], we plan to assign attenuation coefficients inside the lung models based on local 4-D averages of the transmission image data. This local averaging in 4-D neighborhoods classified as lung will also help to mitigate the effects of misclassifying soft tissue as lung, the predominant type of error seen in our 3-D segmentations obtained using the $11\times11\times7$ second directional derivative operator.

VI. Acknowledgments

This work was supported in part by the National Heart, Lung, and Blood Institute of the U.S. Department of Health and Human Services under grant HL25840; and, in part by the Director, Office of Energy Research, Office of Health and Environmental Research, Medical Applications and Biophysical Research Division of the U.S. Department of Energy under contract DE-AC03-76SF00098.

VII. References

[1] M M Ter-Pogossian, S R Bergmann, and B E Sobel. Influence of cardiac and respiratory motion on tomographic reconstructions of the heart: Implications for quantitative nuclear cardiology. *J Comput Assist Tomogr*, 6(6):1148–1155, 1982.

[2] S-C Huang, E J Hoffman, M E Phelps, and D E Kuhl. Quantitation in positron emission computed tomography: 2. Effects of inaccurate attenuation correction. *J Comput Assist Tomogr*, 3(6):804–814, 1979.

[3] M E McCord, S L Bacharach, R O Bonow, V Dilsizian, A Cuocolo, and N Freedman. Misalignment between PET transmission and emission scans: Its effect on myocardial imaging. *J Nucl Med*, 33(6):1209–1214, 1992.

[4] J L R Andersson, B E Vagnhammar, and H Schneider. Accurate attenuation correction despite movement during PET imaging. *J Nucl Med*, 36(4):670–678, 1995.

[5] J O Fredrickson, H Wegmüller, R J Herfkens, and N J Pelc. Simultaneous temporal resolution of cardiac and respiratory motion in MR imaging. *Radiology*, 195:169–175, 1995.

[6] Y Wang, S J Riederer, and R L Ehman. Respiratory motion of the heart: Kinematics and the implications for the spatial resolution in coronary imaging. *Magn Reson Med*, 33(5):713–719, 1995.

[7] T F Budinger, G J Klein, J H Reed, K M Brennan, and R H Huesman. Compensation for respiratory motion in cardiac PET — a feasibility study. *J Nucl Med*, 37(5):130P–131P, 1996.

[8] S-C Huang, R E Carson, M E Phelps, E J Hoffman, H R Schelbert, and D E Kuhl. A boundary method for attenuation correction in positron computed tomography. *J Nucl Med*, 22(7):627–637, 1981.

[9] E Z Xu, N A Mullani, K L Gould, and W L Anderson. A segmented attenuation correction for PET. *J Nucl Med*, 32(1):161–165, 1991.

[10] S R Meikle, M Dahlbom, and S R Cherry. Attenuation correction using count-limited transmission data in positron emission tomography. *J Nucl Med*, 34(1):143–150, 1993.

[11] M Xu, P D Cutler, and W K Luk. Adaptive, segmented attenuation correction for whole-body PET imaging. *IEEE Trans Nucl Sci*, 43(1):331–336, 1996.

[12] S K Yu and C Nahmias. Segmented attenuation correction using artificial neural networks in positron tomography. *Phys Med Biol*, 41:2189–2206, 1996.

[13] V R Algazi, B W Reutter, W L G van Warmerdam, and C C Liu. Three-dimensional image analysis and display by space-scale matching of cross sections. *J Opt Soc Am A*, 6(6):890–899, 1989.

[14] A Goshtasby and D A Turner. Segmentation of cardiac cine MR images for extraction of right and left ventricular chambers. *IEEE Trans Med Imag*, 14(1):56–64, 1995.

[15] G Coppini, R Poli, and G Valli. Recovery of the 3-D shape of the left ventricle from echocardiographic images. *IEEE Trans Med Imag*, 14(2):301–317, 1995.

[16] T-S Pan, M A King, D J de Vries, and M Ljungberg. Segmentation of the body and lungs from Compton scatter and photopeak window data in SPECT: A Monte-Carlo investigation. *IEEE Trans Med Imag*, 15(1):13–24, 1996.

[17] R M Haralick. Digital step edges from zero crossing of second directional derivatives. *IEEE Trans Patt Anal Machine Intell*, PAMI-6(1):58–68, 1984.

[18] J De Vriendt. Accuracy of the zero crossings of the second directional derivative as an edge detector. *Multidim Sys Signal Processing*, 4:227–251, 1993.

[19] S Mallat and S Zhong. Characterization of signals from multiscale edges. *IEEE Trans Patt Anal Machine Intell*, 14(7):710–732, 1992.

[20] A Wallin. Constructing surfaces from CT data. *IEEE Computer Graphics & Applications*, 11(6):28–33, 1991.

IEEE Transactions on Nuclear Science, **44**(6):2473–2476, 1997 (preprint)